Sliding Mode Control of the Modular Multilevel Converter

Qichen Yang
School of Electrical and Computer Engineering
Georgia Institute of Technology
Atlanta, Georgia 30332
Email: qyang45@gatech.edu

Maryam Saeedifard
School of Electrical and Computer Engineering
Georgia Institute of Technology
Atlanta, Georgia 30332
Email: maryam@ece.gatech.edu

***Abstract*—The modular multilevel converter (MMC) has become the most promising converter topology for medium- and high-power applications. In this paper, a sliding mode control (SMC)-based method is proposed for the MMC. Based on analysis of the system dynamics under the proposed control method, control parameter relations and their validity conditions are obtained, which provide guidance for systematic controller design. Compared to the conventional control methods, the proposed SMC-based method provides a faster dynamic response. Performance and effectiveness of the proposed control method are demonstrated based on simulation studies in the PSCAD/EMTDC software environment as well as experiments conducted on a laboratory prototype.**

I. Introduction

The modular multilevel converter (MMC) has become the most promising converter topology for medium- and high-power applications [1]–[4]. In the technical literatures, control methods based on linear controllers, e.g., proportional-integral (PI) and proportional-resonant (PR) controllers, have been proposed to control the MMC [1], [5]–[10]. In addition, control methods based on nonlinear controllers are also proposed [11]–[15], which suffer from large computation loads and/or dependence on exact system models. In this paper, a sliding mode control (SMC)-based method is proposed for the MMC, which provides a faster dynamic response and better robustness compared with the conventional methods. Based on analysis of a wide range of the system dynamics under the proposed control method, control parameter relations and their validity conditions are obtained, which provide guidance for systematic controller design. In addition, the SMC-based control method can be incorporated into the conventional control method to combine the advantages of both the SMC- and conventional PI-based control methods. Effectiveness of the SMC-based control method is verified based on simulation studies in the PSCAD/EMTDC software environment as well as experiments conducted on a laboratory prototype.

II. Dynamics of the Modular Multilevel Converter

The circuit diagram of a three-phase MMC is shown in Fig. 1. The MMC consists of two arms per phase where each arm is comprised of N series-connected, nominally identical

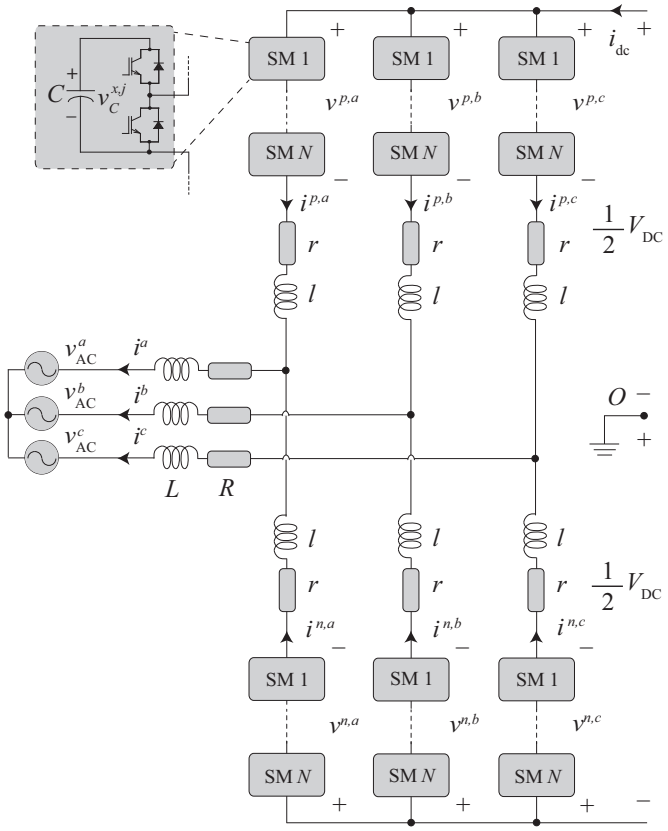

Fig. 1. Circuit diagram of the DC-AC MMC.

half-bridge (HB) SMs and a series-connected arm inductor. Dynamics of the MMC can be summarized by [16], [17]

$$\begin{aligned}
&\tfrac{1}{2}V_{\rm DC} - n^{p,j}v_C^{p,j} - ri^{p,j} - l\tfrac{di^{p,j}}{dt} - Ri^{j} - L\tfrac{di^{j}}{dt} \\
&\qquad - \left(V_{\rm AC}\sin(\theta-\phi^j) + v_{\rm ac,com}\right) = 0, \\
&-\tfrac{1}{2}V_{\rm DC} - n^{n,j}v_C^{n,j} - ri^{n,j} - l\tfrac{di^{n,j}}{dt} - Ri^{j} - L\tfrac{di^{j}}{dt} \\
&\qquad - \left(V_{\rm AC}\sin(\theta-\phi^j) + v_{\rm ac,com}\right) = 0, \\
&C\tfrac{dv_C^{p,j}}{dt} = \tfrac{n^{p,j}}{N}i^{p,j}, \\
&C\tfrac{dv_C^{n,j}}{dt} = -\tfrac{n^{n,j}}{N}i^{n,j},
\end{aligned} \tag{1}$$

where $n^{x,j}$, $v_C^{x,j}$, and $i^{x,j}$ represent the number of inserted SMs, averaged SM capacitor voltage, and arm current in the

978-1-5386-1180-7/18/$31.00 ©2018 IEEE

x ($x = p, n$) arm of phase j ($j = a, b, c$), respectively, $v_{\mathrm{ac,com}}$ is the common-mode component of the AC-side terminal voltages of the MMC, V_{DC} is the DC-link voltage, V_{AC} is the peak value of v_{AC}^{j}, i^{j} is the phase j current, θ is the phase angle of v_{AC}^{a}, and ϕ^{j} is the initial phase angle of v_{AC}^{j}. Generally, the control inputs are obtained based on

$$\begin{aligned} n^{p,j}v_C^{p,j} - n^{n,j}v_C^{n,j} &\approx \left(n^{p,j} - n^{n,j}\right)V_C^{\mathrm{ref}} \\ &\triangleq f(\cdot) + h_{\mathrm{fw,com}}(\cdot), \\ n^{p,j}v_C^{p,j} + n^{n,j}v_C^{n,j} &\approx \left(n^{p,j} + n^{n,j}\right)V_C^{\mathrm{ref}} \\ &\triangleq g(\cdot) + h_{\mathrm{fw,dif}}, \end{aligned} \tag{2}$$

where V_C^{ref} is the SM capacitor voltage reference, $f(\cdot)$ and $g(\cdot)$ are functions to control the ac-side currents and the circulating currents of the MMC, respectively, $h_{\mathrm{fw,com}}(\cdot)$ and $h_{\mathrm{fw,dif}}$ are feed-forward components to control the ac-side currents and the circulating currents of the MMC. Common- and differential-mode components are defined by:

$$\begin{bmatrix} z_{\mathrm{com}}^{j} \\ z_{\mathrm{dif}}^{j} \end{bmatrix} \triangleq \frac{1}{2}\begin{bmatrix} 1 & 1 \\ 1 & -1 \end{bmatrix}\begin{bmatrix} z^{p,j} \\ z^{n,j} \end{bmatrix}, \tag{3}$$

where $z^{x,j}$ is a general designation for $i^{x,j}$, $v^{x,j}$, $v_C^{x,j}$ and $n^{x,j}$, z_{com}^{j} is common-mode component of $z^{x,j}$, and z_{dif}^{j} is differential-mode component of $z^{x,j}$. Based on (3), i_{com}^{j} is half of i^{j}. Substituting (2) and (3) for $i^{x,j}$, $n^{x,j}$, and $v_C^{x,j}$ in (1) yields

$$\begin{aligned} &\frac{d}{d\theta}\begin{bmatrix} i_{\mathrm{com}}^{j} \\ i_{\mathrm{dif}}^{j} \\ v_{C,\mathrm{com}}^{j} \\ v_{C,\mathrm{dif}}^{j} \end{bmatrix} \\ &= \begin{bmatrix} A_{11} & A_{12} \\ A_{21} & A_{22} \end{bmatrix}\begin{bmatrix} i_{\mathrm{com}}^{j} \\ i_{\mathrm{dif}}^{j} \\ v_{C,\mathrm{com}}^{j} \\ v_{C,\mathrm{dif}}^{j} \end{bmatrix} - \frac{1}{2\omega}\begin{bmatrix} v_{\mathrm{AC}}^{j}\big/L_{\mathrm{AC}} \\ -V_{\mathrm{dc}}/l \\ 0 \\ 0 \end{bmatrix}. \end{aligned} \tag{4}$$

Matrices in (4) are

$$\begin{aligned} A_{11} &= \begin{bmatrix} -\frac{R_{\mathrm{AC}}}{\omega L_{\mathrm{AC}}} & 0 \\ 0 & -\frac{r}{\omega l} \end{bmatrix}, \\ A_{12} &= \begin{bmatrix} -\frac{n_{\mathrm{dif}}^{j}}{\omega L_{\mathrm{AC}}} & \frac{n_{\mathrm{com}}^{j}}{\omega L_{\mathrm{AC}}} \\ \frac{n_{\mathrm{com}}^{j}}{\omega l} & -\frac{n_{\mathrm{dif}}^{j}}{\omega l} \end{bmatrix}, \\ A_{21} &= \frac{1}{\omega NC}\begin{bmatrix} n_{\mathrm{dif}}^{j} & -n_{\mathrm{com}}^{j} \\ -n_{\mathrm{com}}^{j} & n_{\mathrm{dif}}^{j} \end{bmatrix}, \\ A_{22} &= 0, \end{aligned} \tag{5}$$

where

$$n_{\mathrm{dif}}^{j} = \frac{f(\cdot)+h_{\mathrm{fw,com}}(\cdot)}{2V_C^{\mathrm{ref}}}, \tag{6a}$$

$$n_{\mathrm{com}}^{j} = \frac{g(\cdot)+h_{\mathrm{fw,dif}}}{2V_C^{\mathrm{ref}}}, \tag{6b}$$

ω is angular frequency of the AC source, L_{AC} is $2L + l$, and R_{AC} is $2R + r$.

III. The Proposed Sliding Mode Control

In the proposed SMC-based control method, common- and differential-mode currents are actively controlled and two control structures are designed for each actively-controlled variable. The two control structures are applied alternatively for a certain time length, i.e., Δt, to force the corresponding variable to slide along the boundary of the two structures within a hysteresis range, i.e., $\pm\Delta i_{\mathrm{com}}^{j}$ or $\pm\Delta i_{\mathrm{dif}}^{j}$.

A. Single-Phase MMC

Since single-phase MMC has only one phase, the superscript j of variables are removed in this sub-section III-A. To control i_{com} and i_{dif} in a single-phase MMC, each of $f(\cdot)$ and $g(\cdot)$ in (2) corresponds to two structures, i.e.,

$$f(\cdot) = \begin{cases} F, & \text{if } \ i_{\mathrm{com}} > i_{\mathrm{com}}^{\mathrm{ref}} \\ -F, & \text{if } \ i_{\mathrm{com}} < i_{\mathrm{com}}^{\mathrm{ref}} \end{cases}, \tag{7a}$$

$$g(\cdot) = \begin{cases} G, & \text{if } \ i_{\mathrm{dif}} > i_{\mathrm{dif}}^{\mathrm{ref}} \\ -G, & \text{if } \ i_{\mathrm{dif}} < i_{\mathrm{dif}}^{\mathrm{ref}} \end{cases}, \tag{7b}$$

where $i_{\mathrm{com}}^{\mathrm{ref}}$ and $i_{\mathrm{dif}}^{\mathrm{ref}}$ are references of i_{com}^{j} and i_{dif}^{j}, F is commanded magnitude of voltage to control the ac-side currents, and G is commanded magnitude of voltage to control the circulating currents. Based on (7), the two structures within each pair alternate based on comparison between the actively-controlled current and its reference. Besides, to generate n_{com}^{j} and n_{dif}^{j}, the feed-forward components in (2) are

$$h_{\mathrm{fw,com}}(\cdot) = -V_{\mathrm{AC}}\sin(\theta), \tag{8a}$$

$$h_{\mathrm{fw,dif}} = -V_{\mathrm{DC}}. \tag{8b}$$

In a well-designed MMC, the magnitude of ripple components of each SM capacitor voltage are regulated within a limited range, i.e.,

$$\begin{aligned} -\Delta v_{C,\mathrm{com}} \le v_{C,\mathrm{com}} - V_C^{\mathrm{ref}} \le \Delta v_{C,\mathrm{com}}, \\ -\Delta v_{C,\mathrm{dif}} \le v_{C,\mathrm{dif}} \le \Delta v_{C,\mathrm{dif}}, \end{aligned} \tag{9}$$

where $\Delta v_{C,\mathrm{com}}$ and $\Delta v_{C,\mathrm{dif}}$ are ripple magnitudes of $v_{C,\mathrm{com}}$ and $v_{C,\mathrm{dif}}$, respectively. Assuming i_{com} is larger than $i_{\mathrm{com}}^{\mathrm{ref}}$ and substituting (6a), (7a), (8), and (9) for n_{com}, n_{dif}, $v_{C,\mathrm{com}}$, and $v_{C,\mathrm{dif}}$ in (4) yields

$$\frac{di_{\mathrm{com}}}{d\theta} = -\frac{R_{\mathrm{AC}}}{\omega L_{\mathrm{AC}}}i_{\mathrm{com}} - \frac{1}{2\omega L_{\mathrm{AC}}}U_{\mathrm{com}}, \tag{10}$$

where U_{com} is the actual magnitude of voltage to control the ac-side currents and is

$$\begin{aligned} &U_{\mathrm{com}} = \\ &\quad F \pm \frac{\Delta v_{C,\mathrm{com}}F}{V_C^{\mathrm{ref}}} \mp \frac{\Delta v_{C,\mathrm{com}}v_{\mathrm{AC}}}{V_C^{\mathrm{ref}}} \mp \frac{\Delta v_{C,\mathrm{dif}}(\pm G + V_{\mathrm{DC}})}{V_C^{\mathrm{ref}}}. \end{aligned} \tag{11}$$

Based on (11), the range of U_{com} is

$$\begin{aligned} U_{\mathrm{com}} &\le U_{\mathrm{com,max}} \\ &\triangleq F + \frac{\Delta v_{C,\mathrm{com}}(F+V_{\mathrm{AC}}) + \Delta v_{C,\mathrm{dif}}(G+V_{\mathrm{DC}})}{V_C^{\mathrm{ref}}}, \\ U_{\mathrm{com}} &\ge U_{\mathrm{com,min}} \\ &\triangleq F - \frac{\Delta v_{C,\mathrm{com}}(F+V_{\mathrm{AC}}) + \Delta v_{C,\mathrm{dif}}(G+V_{\mathrm{DC}})}{V_C^{\mathrm{ref}}}. \end{aligned} \tag{12}$$

Since Δt is much smaller than the line period, $U_{\rm com}$ can be regarded as a constant when a control structure is applied. Solving (10) for $i_{\rm com}$ yields

$$\begin{aligned} i_{\rm com}(\theta) = i_{\rm com}(\theta_0)\exp\left(-\tfrac{R_{\rm AC}}{\omega L_{\rm AC}}(\theta-\theta_0)\right) \\ + \tfrac{U_{\rm com}}{R_{\rm AC}}\left(\exp\left(-\tfrac{R_{\rm AC}}{\omega L_{\rm AC}}(\theta-\theta_0)\right)-1\right), \end{aligned} \tag{13}$$

where θ_0 is the phase angle θ at the moment of alternating control structure. At the beginning and end of a period of applying a control structure,

$$\begin{aligned} i_{\rm com}(\theta_0+\Delta\theta) = i_{\rm com}^{\rm ref}(\theta_0+\Delta\theta) - \Delta i_{\rm com}, \\ i_{\rm com}(\theta_0) = i_{\rm com}^{\rm ref}(\theta_0) + \Delta i_{\rm com}, \end{aligned} \tag{14}$$

where $\Delta i_{\rm com}$ is the ripple magnitude of $i_{\rm com}$ and $\Delta\theta$ is $\omega\Delta t$. By substituting (14) for $i_{\rm com}(\theta)$ and $i_{\rm com}(\theta_0)$ into (13), and reorganizing the equation, (13) can be transformed into

$$\exp\left(-\tfrac{R_{\rm AC}}{\omega L_{\rm AC}}\Delta\theta\right) = \tfrac{R_{\rm AC}\left(i_{\rm com}^{\rm ref}(\theta_0+\Delta\theta)-\Delta i_{\rm com}\right)+U_{\rm com}}{R_{\rm AC}(i_{\rm com}^{\rm ref}(\theta_0)+\Delta i_{\rm com})+U_{\rm com}}. \tag{15}$$

In (15), $i_{\rm com}^{\rm ref}$ is

$$i_{\rm com}^{\rm ref}(\theta) = I_{\rm com}^{\rm ref}\sin\left(\theta+\phi_{I,\rm com}^{\rm ref}\right), \tag{16}$$

where $I_{\rm com}^{\rm ref}$ and $\phi_{I,\rm com}^{\rm ref}$ are the magnitude and phase angle of $i_{\rm com}^{\rm ref}$, respectively. Linearizing $\exp\left(-\tfrac{R_{\rm AC}}{\omega L_{\rm AC}}\Delta\theta\right)$ around $\Delta\theta\approx 0$ in the left side of (15) yields

$$\exp\left(-\frac{R_{\rm AC}}{\omega L_{\rm AC}}\Delta\theta\right) \approx 1-\frac{R_{\rm AC}}{\omega L_{\rm AC}}\Delta\theta. \tag{17}$$

Linearizing $\sin\left(\theta+\phi_{I,\rm com}^{\rm ref}\right)$ in (16) around $\theta\approx\theta_0$ yields

$$i_{\rm com}^{\rm ref}(\theta_0+\Delta\theta) \approx i_{\rm com}^{\rm ref}(\theta_0) + I_{\rm com}^{\rm ref}\cos\left(\theta_0+\phi_{I,\rm com}^{\rm ref}\right)\Delta\theta. \tag{18}$$

Substituting (16), (17), and (18) in (15) and simplifying, relation among F, Δt, and $\Delta i_{\rm com}$ can be obtained as:

$$\begin{aligned} \Delta t &= \tfrac{2\Delta i_{\rm com}}{\frac{U_{\rm com}}{L_{\rm AC}}+\omega I_{\rm com}^{\rm ref}\cos\left(\theta_0+\phi_{I,\rm com}^{\rm ref}\right)+\frac{R_{\rm AC}}{L_{\rm AC}}i_{\rm com}^{\rm ref}(\theta_0)} \\ &\approx \tfrac{2L_{\rm AC}\Delta i_{\rm com}}{U_{\rm com}} \\ &\approx \tfrac{2L_{\rm AC}\Delta i_{\rm com}}{F}. \end{aligned} \tag{19}$$

Considering the validity conditions of all the approximations from (10) to (19), the validity conditions of (19) are derived as:

$$\tfrac{1}{6}\Delta\theta^3 \ll 1, \tag{20a}$$

$$\tfrac{1}{2}\left(\tfrac{R_{\rm AC}}{\omega L_{\rm AC}}\Delta\theta\right)^2 \ll 1, \tag{20b}$$

$$U_{\rm com,min} \gg I_{\rm com}^{\rm ref}\sqrt{(\omega L_{\rm AC})^2+(R_{\rm AC})^2}, \tag{20c}$$

$$V_C^{\rm ref} \gg \Delta v_{C,\rm com}(F+V_{\rm AC}) + \Delta v_{C,\rm dif}(G+V_{\rm DC}), \tag{20d}$$

where (20a) and (20b) keep the validity of linearization from (15) to (19) and (20c) and (20d) support the simplification of the denominator of (19).

Similarly, relation among G, Δt, and ripple magnitude of $i_{\rm dif}$, i.e., $\Delta i_{\rm dif}$ is

$$\begin{aligned} \Delta t &= \tfrac{2l\Delta i_{\rm dif}}{r\left(i_{\rm dif}^{\rm ref}+\Delta i_{\rm dif}\right)+U_{\rm dif}} \\ &\approx \tfrac{2l\Delta i_{\rm dif}}{U_{\rm djf}} \\ &\approx \tfrac{2l\Delta i_{\rm dif}}{G}. \end{aligned} \tag{21}$$

The validity conditions of (21) are

$$\begin{aligned} \tfrac{1}{2}\left(\tfrac{r}{\omega l}\Delta\theta\right)^2 \ll 1, \\ U_{\rm dif,min} \gg r i_{\rm dif}^{\rm ref} \\ V_C^{\rm ref} \gg \Delta v_{C,\rm com}(G+V_{\rm DC}) + \Delta v_{C,\rm dif}(F+V_{\rm AC}), \end{aligned} \tag{22}$$

where $U_{\rm dif}$ is actual magnitude of voltage to control the circulating currents and its minimum value is

$$\begin{aligned} U_{\rm dif,min} \\ = G - \tfrac{\Delta v_{C,\rm com}(G+V_{\rm DC})+\Delta v_{C,\rm dif}(F+V_{\rm AC})}{V_C^{\rm ref}}. \end{aligned} \tag{23}$$

B. Three-Phase MMC

In a three-phase MMC, the three-phase circulating currents are independent. Therefore, $g(\cdot)$ and $h_{\rm fw,dif}(\cdot)$ of a three-phase MMC are the same with those of a single-phase MMC in (7). However, dynamics of three-phase $i_{\rm com}^j$ is different from that of a single-phase MMC as the three-phase currents are not independent. Therefore, $f(\cdot)$ and $h_{\rm fw,com}(\cdot)$ of a three-phase MMC need to be modified based on the dq transformation by

$$\begin{bmatrix} n_{\rm dif}^a \\ n_{\rm dif}^b \\ n_{\rm dif}^c \end{bmatrix} = \frac{1}{2V_C^{\rm ref}}\begin{bmatrix} f^a(\cdot) \\ f^b(\cdot) \\ f^c(\cdot) \end{bmatrix} + \frac{1}{2V_C^{\rm ref}}\begin{bmatrix} h_{\rm fw,com}^a \\ h_{\rm fw,com}^b \\ h_{\rm fw,com}^c \end{bmatrix}, \tag{24}$$

where

$$\begin{aligned} \begin{bmatrix} f^a(\cdot) \\ f^b(\cdot) \\ f^c(\cdot) \end{bmatrix} &= -T^{-1}\begin{bmatrix} f^q(\cdot) \\ f^d(\cdot) \end{bmatrix}, \\ \begin{bmatrix} h_{\rm fw,com}^a \\ h_{\rm fw,com}^b \\ h_{\rm fw,com}^c \end{bmatrix} &= -2\begin{bmatrix} v_{\rm AC}^a \\ v_{\rm AC}^b \\ v_{\rm AC}^c \end{bmatrix} \\ &\quad - \tfrac{4\sqrt{3}\omega L_{\rm AC}}{3}\begin{bmatrix} 0 & -1 & 1 \\ 1 & 0 & -1 \\ -1 & 1 & 0 \end{bmatrix}\begin{bmatrix} i_{\rm com}^a \\ i_{\rm com}^b \\ i_{\rm com}^c \end{bmatrix}. \end{aligned} \tag{25}$$

In (25),

$$\begin{aligned} f^q(\cdot) &= \begin{cases} F, & i^q > i^{q,\rm ref} \\ -F, & i^q < i^{q,\rm ref} \end{cases}, \\ f^d(\cdot) &= \begin{cases} F, & i^d > i^{d,\rm ref} \\ -F, & i^d < i^{d,\rm ref} \end{cases}, \end{aligned} \tag{26}$$

where $i_{\rm com}^\xi$ is the ξ-axis component of three-phase $i_{\rm com}^j$ ($\xi = q, d$) and $i_{\rm com}^{\xi,\rm ref}$ is the reference of $i_{\rm com}^\xi$.

Common- and differential-mode ripple components, i.e., $\Delta v_{C,\rm com}^j$ and $\Delta v_{C,\rm dif}^j$ are significantly smaller than $V_C^{\rm ref}$ in a well-designed MMC. Therefore, based on (4) and (26), if $i_{\rm com}^q$ and $i_{\rm com}^d$ are both larger than their references, i.e., $I_{\rm com}^{q,\rm ref}$ and $I_{\rm com}^{d,\rm ref}$, the dynamics of $i_{\rm com}^a$ becomes

$$\begin{aligned} \tfrac{d}{d\theta}i_{\rm com}^a = -\tfrac{R_{\rm AC}}{\omega L_{\rm AC}}i_{\rm com}^a + \tfrac{\sqrt{3}}{3}\left(-i_{\rm com}^b+i_{\rm com}^c\right) \\ - \tfrac{F}{2\omega L_{\rm AC}}\left(\cos(\theta)+\sin(\theta)\right), \end{aligned} \tag{27}$$

which can be decoupled into

$$\begin{array}{l}\frac{d}{d\theta}i_{\rm com}^{d}=-\frac{R_{\rm AC}}{\omega L_{\rm AC}}i_{\rm com}^{d}-\frac{F}{2\omega L_{\rm AC}},\\ \frac{d}{d\theta}i_{\rm com}^{q}=-\frac{R_{\rm AC}}{\omega L_{\rm AC}}i_{\rm com}^{q}-\frac{F}{2\omega L_{\rm AC}}.\end{array}\tag{28}$$

Solving for $i_{\rm com}^{\xi}$ based on (28) and simplifying the results based on approximations result yields

$$\Delta\theta\approx\frac{2\omega L_{\rm AC}\Delta i_{\rm com}^{\xi}}{F}.\tag{29}$$

The validity conditions of (29) are

$$\begin{array}{c}\frac{1}{2}\left(\frac{R_{\rm AC}}{\omega L_{\rm AC}}\Delta\theta\right)^{2}\ll 1,\\ F\gg R_{\rm AC}\left(I_{\rm com}^{\xi,\rm ref}+\Delta i_{\rm com}^{\xi}\right),\\ V_{C}^{\rm ref}\gg\Delta v_{C,\rm dif},\\ V_{C}^{\rm ref}\gg\Delta v_{C,\rm com}.\end{array}\tag{30}$$

C. Fixed-Frequency Comparison

To limit the frequency variation of gating signals, $i_{\rm com}^{\xi}$ and $i_{\rm dif}^{j}$ are compared with their references at a fixed frequency, i.e., $f_{\rm S,en}$. Since the fixed-frequency comparison could create a time-variable asymmetrical hysteresis range, the hysteresis range can be twice of those in (21) and (29). Therefore, considering (21) and (29) as well as the variation of AC source voltages, the fixed frequency is designed based on

$$f_{\rm S,en}\geq\max\left\{\frac{\omega V_{\rm AC}}{V_{C}^{\rm ref}},\frac{F}{L_{\rm AC}\Delta i_{\rm com}^{\xi}},\frac{G}{l\Delta i_{\rm dif}^{j}}\right\}.\tag{31}$$

Subsequent to determination of $f_{\rm S,en}$, $\Delta i_{\rm com}^{\xi}$ and $\Delta i_{\rm dif}^{j}$ are

$$\begin{array}{l}\Delta i_{\rm com}^{\xi}=\frac{F}{f_{\rm S,en}L_{\rm AC}},\\ \Delta i_{\rm dif}^{j}=\frac{G}{f_{\rm S,en}l}.\end{array}\tag{32}$$

The implementation block diagram of the proposed SMC-based control method is summarized in Fig. 2.

D. Comparison with the Conventional PI-based Control Strategy

In the conventional PI-based control strategy, the integral gain, i.e., $K_{\rm I}$ is designed based on $R_{\rm AC}$, $L_{\rm AC}$, and the proportional gain, i.e., $K_{\rm P}$:

$$R_{\rm AC}/L_{\rm AC}=K_{\rm I}/K_{\rm P},\tag{33}$$

to cancel a pole at $s=-R_{\rm AC}/L_{\rm AC}$ [18]. Based on this principle, zero-state response of $i_{\rm com}^{\xi}$ for a step change of its reference, i.e., $i_{\rm com}^{\xi,\rm ref}$ from 0 to a new reference, i.e., $I_{\rm com}^{\xi,\rm ref,new}$ is illustrated in (34), while the response of $i_{\rm com}^{\xi}$ under the proposed SMC-based control is illustrated in (35).

$$i_{\rm com}^{\xi}=\left(1-\exp\left(-\frac{2K_{\rm P}t}{L_{\rm AC}}\right)\right)I_{\rm com}^{\xi,\rm ref,new}\tag{34}$$

$$i_{\rm com}^{\xi}\approx\frac{Ft}{2L_{\rm AC}}\tag{35}$$

To prevent over-modulation under a step-up change of $i_{\rm com}^{q,\rm ref}$ from a previous reference, i.e., $I_{\rm com}^{q,\rm ref,pre}$ to $I_{\rm com}^{q,\rm ref,new}$, parameters in the PI-based control method and the SMC-based control method are constrained by the following upper limits:

$$\begin{aligned}&F_{\max}^{q}\\ &\approx\sqrt{\left(0.575V_{\rm DC}\right)^{2}-\left(F^{d}\right)^{2}}-\left(V_{\rm AC}^{q}-\omega L_{\rm AC}I_{\rm com}^{d,\rm ref}\right),\end{aligned}\tag{36a}$$

$$K_{\rm P,max}\approx\frac{\sqrt{\left(0.575V_{\rm DC}\right)^{2}-\left(V_{\rm tmn}^{d,\rm ref}\right)^{2}}-\left(V_{\rm AC}^{q}-\omega L_{\rm AC}I_{\rm com}^{d,\rm ref}\right)}{I_{\rm com}^{q,\rm ref,new}-I_{\rm com}^{q,\rm ref,pre}},\tag{36b}$$

where F^{ξ} is the magnitude of voltage to control $i_{\rm com}^{\xi}$ in the SMC-based control method, $V_{\rm AC}^{\xi}$ is the ξ-axis component of three-phase AC source voltages, and $V_{\rm tmn}^{\xi}$ is ξ-axis component of AC-side terminal voltages of the MMC. The value of $V_{\rm tmn}^{\xi}$ is the

$$V_{\rm tmn}^{d,\rm ref}=\left(R_{\rm AC}I_{\rm com}^{d,\rm ref}+\omega L_{\rm AC}I_{\rm com}^{q,\rm ref,pre}\right).\tag{37}$$

Based on (34), as $i_{\rm com}^{\xi}$ reaches $I_{\rm com}^{\xi,\rm ref,new}$, the zero-approaching speed of the error between $i_{\rm com}^{\xi}$ and $I_{\rm com}^{\xi,\rm ref,new}$ decreases under the PI-based control method. On the other hand, based on (35), under the proposed SMC-based control method, the error decreasing speed is a constant, which is not impacted by the difference between $i_{\rm com}^{\xi}$ and its reference. Meanwhile, based on (36b), $K_{\rm P,max}$ is inversely proportional to the step change magnitude, which also limits the speed of the dynamic response of the PI-based control with large $\Delta I_{\rm com}^{\xi}$. On the contrary, $F_{\max}$ is not impacted by the step change magnitude. Therefore, the proposed SMC-based control can provide a faster dynamic response speed over the conventional PI-based control.

In addition, in the PI-based control, effective pole cancellation at $s=-R_{\rm AC}/L_{\rm AC}$ and prevention from over-modulation both depend on exact parameters and precise model of the system, which are hard to be obtained in practice. However, in the proposed SMC-based control, alternation of control structures is based on comparison between actively-controlled variables and their references, which does not require precise system parameters.

Although a large F can potentially increase the speed of response during transients, the large excitation causes large high-frequency harmonics during steady state. To solve the problem, an enhanced SMC-based control method with variable F is proposed:

$$F=\left\{\begin{array}{ll}F_{\max}, & \left|i_{\rm com}^{\xi}-i_{\rm com}^{\xi,\rm ref}\right|>i_{\rm com}^{\xi,\rm thd}\\ F_{\rm steady}, & \left|i_{\rm com}^{\xi}-i_{\rm com}^{\xi,\rm ref}\right|\leq i_{\rm com}^{\xi,\rm thd}\end{array}\right.,\tag{38}$$

where $F_{\max}$ is maximum of F, $F_{\rm steady}$ is the magnitude of voltage in steady state, and $i_{\rm com}^{\xi,\rm thd}$ is a threshold to determine the magnitude of excitation ($F_{\max}$ or $F_{\rm steady}$). In (38), $i_{\rm com}^{\xi,\rm thd}$ is designed by

$$i_{\rm com}^{\xi,\rm thd}\triangleq\eta\frac{F_{\rm steady}}{L_{\rm AC}f_{\rm S,en}}.\tag{39}$$

Besides, $F_{\max}$ is designed by (36a), $F_{\rm steady}$ is designed based on (32), and η is slightly larger than 1.

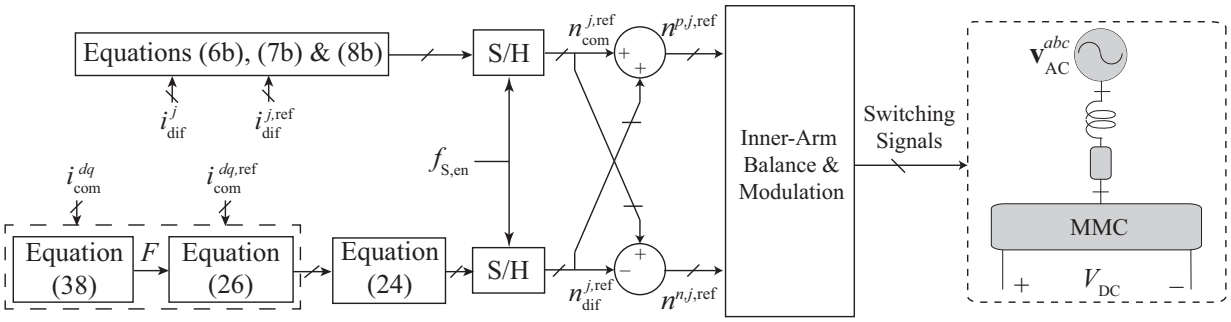

Fig. 2. Block diagram of the proposed SMC-based control method.

Since in the PI-based control method, the magnitude of ripple components during steady state is smaller, a hybrid control method based on combination of the SMC-based and the PI-based control methods is proposed, which is illustrated in Fig. 3. In the hybrid control method, small steady state voltage ripple magnitude under the PI-based control method and excellent dynamic response of the SMC-based control method are combined together.

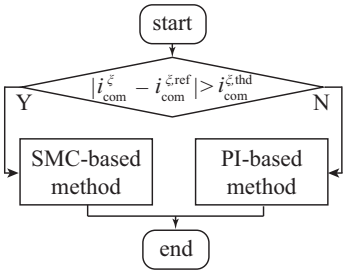

Fig. 3. Hybrid control of the MMC based on combination of PI- and SMC-based strategies.

IV. Simulation Results

To demonstrate performance and effectiveness of the proposed control method, a three-phase MMC is simulated in the PSCAD/EMTDC software environment. Parameters of the study system are listed in Table I and the control system is designed based on (31), (36), and (38). Steady-state waveforms under the proposed SMC-based control method are provided in Fig. 4, where the setpoints of real and reactive power are 120 MW and 80 MVAr, respectively. Based on Figs. 4(a)-(c), three-phase line currents, circulating currents, and SM capacitor voltages are well regulated under the proposed method. Figs. 4(d)-(f) illustrate $i^{\xi}_{\rm com}$ and $i^{j}_{\rm dif}$ within one line cycle. The magnitudes of ripple components of $i^{\xi}_{\rm com}$ and $i^{j}_{\rm dif}$ are closely matched with their theoretical values in (32), as shown in Table II. Dynamic response of the MMC to a step change of $i^{q,\rm ref}$ under the proposed SMC-based method is presented in Fig. 6, where $i^{q,\rm ref}$ steps up from 0 to 15 MW at $t = 0.27$ s and $i^{d,\rm ref}$ remains to be at -10 MVAr. Dynamic response of i^{q} under the proposed SMC-based control method is compared with the one under PI-based control method in Fig. 6(a), where the PI-based controller is designed based on (33) and (36). As illustrated in Fig. 6(a), the proposed SMC-based control method can provide a faster dynamic response than the conventional PI-based control method. In addition, Fig. 6(b) shows that i^{d} remains to be decoupled from i^{q} during the transient under the proposed SMC-based control method. Therefore, the three-phase line currents are well-regulated, as illustrated in Fig. 6(c). In addition, Figs. 6(d)-(f) show that the currents of the six arms are controlled as expected, where the second-order components are suppressed. As illustrated in Figs. 6(g)-(i), the average SM capacitor voltages of the six arms are also well-regulated.

TABLE I
PARAMETERS OF THE STUDY SYSTEM

Rating Value	Value
AC system nominal voltage $V_{\rm in,ll,rms}$	30 kV
Nominal frequency of ac system f	60 Hz
DC link voltage $V_{\rm DC}$	60 kV
Reference of SM capacitor voltage $V_C^{\rm ref}$	3 kV
MMC Parameter	**Value**
L	7 mH
R	0.03 Ω
Series-connected inductance l	6 mH
Resistance of series-connected inductor r	0.02 Ω
Number of SMs in each cluster N	20
Submodule capacitor C	14000 μF
Control Parameter	**Value**
$F^{\rm static}$ in (32)	6 kV
G in (32)	6 kV
$f_{\rm S,en}$ in (32)	7.5 kHz

TABLE II
MAGNITUDE OF RIPPLE COMPONENTS OF $i^{\xi}_{\rm com}$ AND $i^{j}_{\rm dif}$

	$i^{d}_{\rm com}$ (i^{d}/2)	$i^{q}_{\rm com}$ (i^{q}/2)	$i^{a}_{\rm dif}$
Simulation-based $\lvert\Delta i\rvert$ (kA)	0.039	0.042	0.105
Theoretical $\lvert\Delta i\rvert$ (kA)	0.04	0.04	0.133

V. Experimental Verification

The proposed SMC-based control method is also verified experimentally. The prototype is shown in Fig. 5 and the parameters are listed in Table III. In the experimental prototype, the DC-side of the three-phase MMC is supplied by a programmable DC power supply while its AC side is connected to a three-phase RL load. The control method

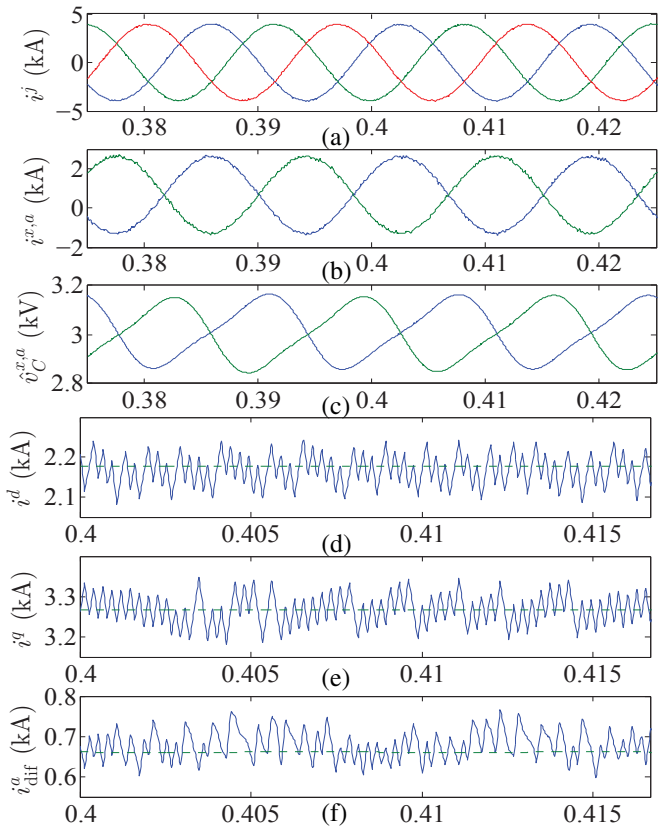

Fig. 4. Steady-state MMC waveforms under the proposed sliding mode control: (a) three-phase line currents, (b) arm current of phase a, (c) SM capacitor voltages of phase a, (d) d-axis component of line currents and its reference, (e) q-axis component of line currents and its reference, and (f) circulating current of phase a and its reference.

Fig. 5. Experiment Setup of the three-phase MMC prototype.

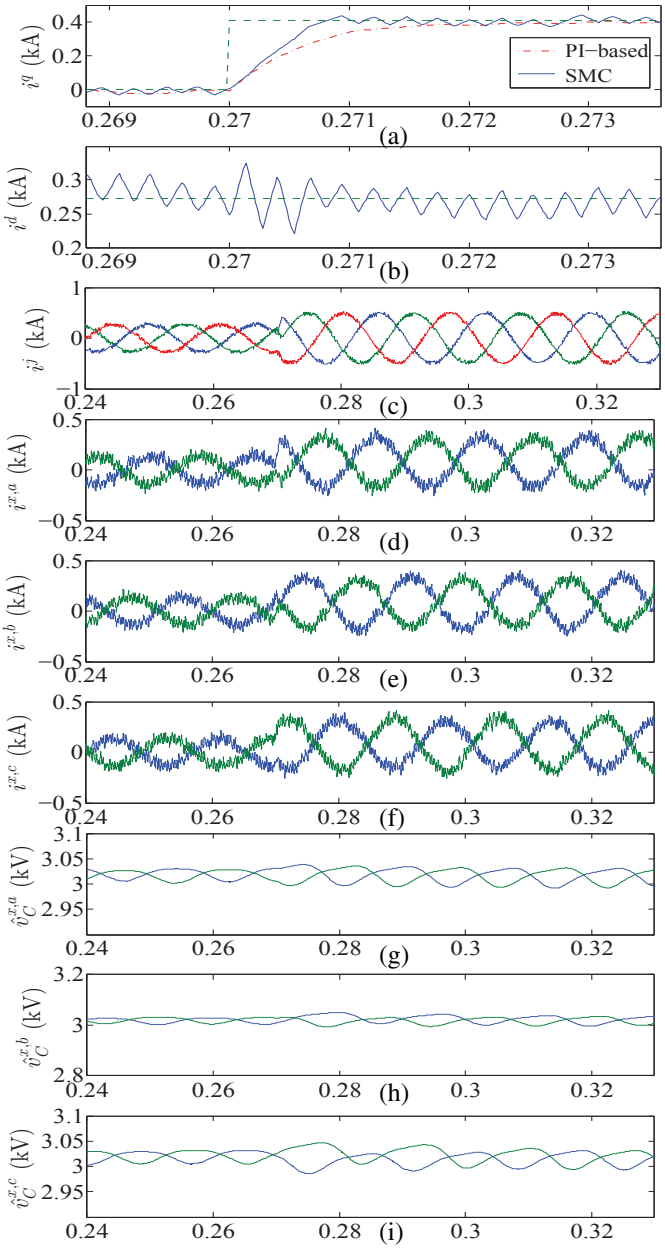

Fig. 6. Response of the MMC to a step change of $i^{q,\text{ref}}$ under the proposed sliding mode control: (a,b) q- and d-axis components of the line currents and their references, (c) three-phase line currents, (d-f) arm currents of phases a, b, and c, and (g-i) SM capacitor voltages of phases a, b, and c.

is implemented in the RT-Lab and OPAL-RT rapid control prototyping tool.

Fig. 7 presents the experimental waveforms under the proposed sliding mode control, where $i^{q,\text{ref}}$ steps up from 1 A to 4 A at $t = 50$ ms while $i^{d,\text{ref}}$ remains to be zero. As illustrated in Figs. 7(a)-(d), the three-phase line currents closely track their references under the sliding mode control. Based on Fig. 7(d), the rise time of i^q is about 1.4 ms, reaching 3.7 A (90 % the $\Delta I^{q,\text{ref}}$) without any overshoot. Figs. 7(e) and (f) present the arm currents and SM capacitor voltages of phase

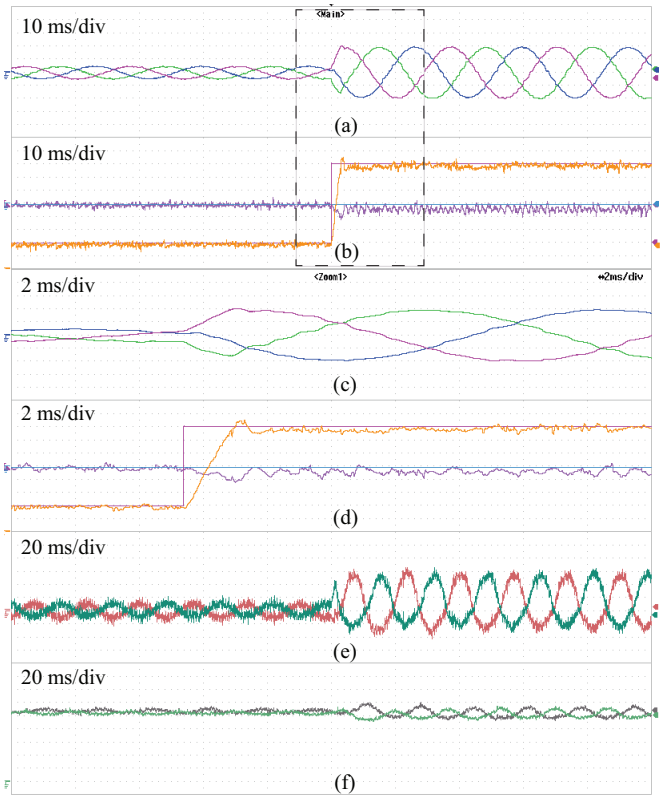

Fig. 7. Experimental MMC waveforms under the proposed SMC-based control method: (a) three-phase line currents, (b) q- and d-axis components of the line currents and their references, (c) zoomed-in three-phase line currents, (d) zoomed-in q- and d-axis components of the line currents and their references, (e) arm currents of phase a, and (f) SM capacitor voltages of phase a.

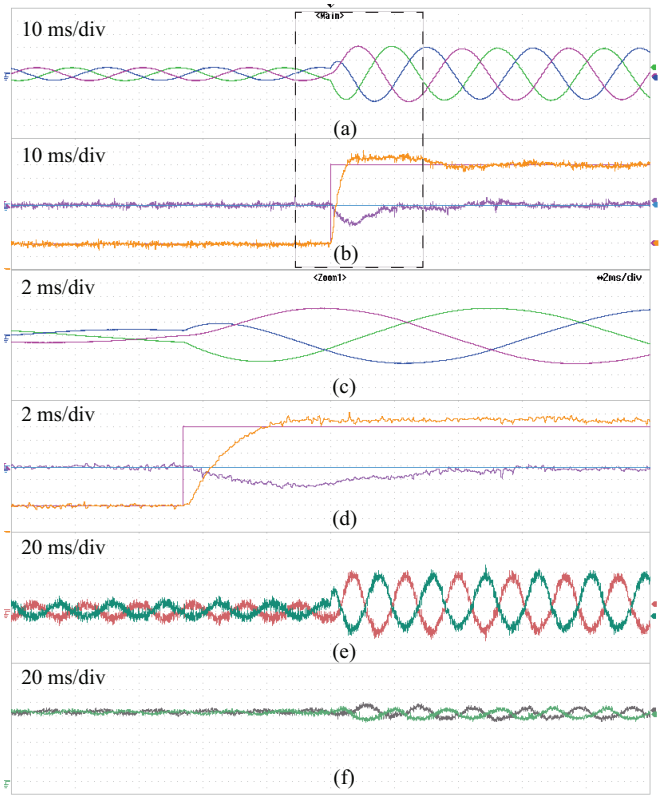

Fig. 8. Experimental MMC waveforms under the conventional PI-based control method: (a) three-phase line currents, (b) q- and d-axis components of the line currents and their references, (c) zoomed-in three-phase line currents, (d) zoomed-in q- and d-axis components of the line currents and their references, (e) arm currents of phase a, and (f) SM capacitor voltages of phase a.

a, which are well controlled during the transient. Fig. 8 presents the corresponding experimental waveforms under the conventional PI-based control with the same scenario, where $i^{q,\mathrm{ref}}$ steps up from 1 A to 4 A. As shown in Fig. 8(d), under the PI-based control, the rise time for i^q is 2.2 ms, which is 57% longer than that under the proposed sliding mode control. This verifies the capability of the proposed SMC-based control method in providing a faster dynamic response over the PI-based one.

VI. Conclusion

This paper proposes a sliding mode controller (SMC) for the MMC. Based on the analysis of the MMC under the proposed SMC-based control method, control parameter relations and their validity conditions are obtained. Compared with PI-based control, the proposed control method is capable of providing a faster dynamic response without compromising the computational effort or requirement for precise system model. Simulation and experimental results are presented to illustrate the salient features of the proposed control method as opposed to the conventional PI-based control method.

TABLE III
PARAMETERS OF THE EXPERIMENTAL SETUP

Quantity	Value
Nominal frequency	60 Hz
DC source voltage V_{DC}	100 V
Load R_{load}	6.7 Ω
Load L_{load}	4.5 mH
Number of SMs per arm N	4
Buffer inductance l	2.5 mH
Submodule capacitor C	1410 μF
Switching frequency f_{sw}	8 kHz

References

[1] S. Debnath, J. Qin, B. Bahrani, M. Saeedifard, and P. Barbosa, "Operation, control, and applications of the modular multilevel converter: A review," *IEEE Trans. Power Electron.*, vol. 30, no. 1, pp. 37–53, Jan 2015.

[2] M. A. Perez, S. Bernet, J. Rodriguez, S. Kouro, and R. Lizana, "Circuit topologies, modeling, control schemes, and applications of modular multilevel converters," *IEEE Trans. on Power Electron.*, vol. 30, no. 1, pp. 4–17, Jan 2015.

[3] S. Allebrod, R. Hamerski, and R. Marquardt, "New transformerless, scalable modular multilevel converters for HVDC-transmission," in *Proc. IEEE PESC*, June 2008, pp. 174–179.

[4] J. Dorn, H. Huang, and D. Retzmann, "A new multilevel voltage-sourced converter topology for HVDC applications," in *Cigre Session*, 2008, pp. B4–304.

[5] K. Sharifabadi, L. Harnefors, H.-P. Nee, S. Norrga, and R. Teodorescu, *Dynamics and Control*. Wiley-IEEE Press, 2016, pp. 133–213.

[6] R. Teodorescu, F. Blaabjerg, M. Liserre, and P. C. Loh, "Proportional-resonant controllers and filters for grid-connected voltage-source converters," *Proc. IEE EPA*, vol. 153, no. 5, pp. 750–762, September 2006.
[7] Q. Tu, Z. Xu, and L. Xu, "Reduced switching-frequency modulation and circulating current suppression for modular multilevel converters," *IEEE Trans. on Power Del.*, vol. 26, no. 3, pp. 2009–2017, July 2011.
[8] G. Konstantinou, J. Pou, S. Ceballos, R. Picas, J. Zaragoza, and V. G. Agelidis, "Control of circulating currents in modular multilevel converters through redundant voltage levels," *IEEE Trans. on Power Electron.*, vol. 31, no. 11, pp. 7761–7769, Nov 2016.
[9] X. Shi, Z. Wang, B. Liu, Y. Liu, L. M. Tolbert, and F. Wang, "Characteristic investigation and control of a modular multilevel converter-based HVDC system under single-line-to-ground fault conditions," *IEEE Trans. on Power Electron.*, vol. 30, no. 1, pp. 408–421, Jan 2015.
[10] X. She, A. Huang, X. Ni, and R. Burgos, "Ac circulating currents suppression in modular multilevel converter," in *Proc. IEEE IECON*, Oct 2012, pp. 191–196.
[11] J. Qin and M. Saeedifard, "Predictive control of a modular multilevel converter for a back-to-back HVDC system," *IEEE Trans. on Power Del.*, vol. 27, no. 3, pp. 1538–1547, July 2012.
[12] M. Vatani, B. Bahrani, M. Saeedifard, and M. Hovd, "Indirect finite control set model predictive control of modular multilevel converters," *IEEE Trans. on Smart Grid*, vol. 6, no. 3, pp. 1520–1529, May 2015.
[13] B. S. Riar, T. Geyer, and U. K. Madawala, "Model predictive direct current control of modular multilevel converters: Modeling, analysis, and experimental evaluation," *IEEE Trans. on Power Electron.*, vol. 30, no. 1, pp. 431–439, Jan 2015.
[14] L. Ben-Brahim, A. Gastli, M. Trabelsi, K. A. Ghazi, M. Houchati, and H. Abu-Rub, "Modular multilevel converter circulating current reduction using model predictive control," *IEEE Trans. on Ind. Electron.*, vol. 63, no. 6, pp. 3857–3866, June 2016.
[15] H. Brnklau, A. Gensior, and J. Rudolph, "A model-based control scheme for modular multilevel converters," *IEEE Trans. on Ind. Electron.*, vol. 60, no. 12, pp. 5359–5375, Dec 2013.
[16] L. Harnefors, A. Antonopoulos, S. Norrga, L. Angquist, and H. P. Nee, "Dynamic analysis of modular multilevel converters," *IEEE Trans. on Ind. Electron.*, vol. 60, no. 7, pp. 2526–2537, July 2013.
[17] D. C. Ludois and G. Venkataramanan, "Simplified terminal behavioral model for a modular multilevel converter," *IEEE Trans. on Power Electron.*, vol. 29, no. 4, pp. 1622–1631, April 2014.
[18] A. Yazdani and R. Iravani, *Grid-Imposed Frequency VSC System: Control in dq-Frame*. Wiley-IEEE Press, 2010, pp. 204–244.